Structure, Vol. 13, 1545–1557, October, 2005, ©2005 Elsevier Ltd All rights reserved. DOI 10.1016/j.str.2005.07.012

Features of Reovirus Outer Capsid Protein μ1 Revealed by Electron Cryomicroscopy and Image Reconstruction of the Virion at 7.0 Å Resolution

Xing Zhang,[1] Yongchang Ji,[2] Lan Zhang,[3] Stephen C. Harrison,[3,4,5] Dan C. Marinescu,[2] Max L. Nibert,[6,*] and Timothy S. Baker[1,7,*]

[1]Department of Biological Sciences
Purdue University
West Lafayette, Indiana 47907

[2]Computer Sciences Department
University of Central Florida
Orlando, Florida 32816

[3]Laboratory of Molecular Medicine

[4]Howard Hughes Medical Institute
Children's Hospital
Boston, Massachusetts 02115

[5]Department of Biological Chemistry and Molecular Pharmacology

[6]Department of Microbiology and Molecular Genetics
Harvard Medical School
Boston, Massachusetts 02115

[7]Department of Chemistry and Biochemistry and Department of Molecular Biology
University of California, San Diego
La Jolla, California 92093

Summary

Reovirus is a useful model for addressing the molecular basis of membrane penetration by one of the larger nonenveloped animal viruses. We now report the structure of the reovirus virion at 7.0 Å resolution as obtained by electron cryomicroscopy and three-dimensional image reconstruction. Several features of the myristoylated outer capsid protein μ1, not seen in a previous X-ray crystal structure of the μ1-σ3 heterohexamer, are evident in the virion. These features appear to be important for stabilizing the outer capsid, regulating the conformational changes in μ1 that accompany perforation of target membranes, and contributing directly to membrane penetration during cell entry.

Introduction

Nonfusogenic mammalian orthoreoviruses (reoviruses), from the genus *Orthoreovirus*, family *Reoviridae*, are a classic system for studies of virus-cell and virus-host interactions in pathogenesis (reviewed in Forrest and Dermody, 2003; Nibert et al., 1991a; Sharpe and Fields, 1985; Tyler et al., 2001). One interesting but poorly understood step in cell entry by reovirus and other nonenveloped viruses is membrane penetration, by which these viruses cross the cellular membrane barrier and enter the cytoplasm to begin infection. The reovirus virion is >850 Å in diameter and comprises two concentric, icosahedral protein capsids surrounding a ten segment, double-stranded (ds) RNA genome. One of the major outer capsid proteins, μ1 (76 kDa, 600 copies per virion), has been implicated in membrane perforation (reviewed in Chandran and Nibert, 2003). The perforation activity is thought to allow a partially uncoated form of the particle to enter the cytoplasm. How μ1 affects this function remains a subject of study, but recent results implicate autolytic release of a myristoylated, amino (N)-terminal fragment of μ1 as one key step (Odegard et al., 2004).

An X-ray crystal structure of μ1 in complex with its "protector" protein σ3 has been determined at 2.8 Å resolution (Liemann et al., 2002). The complex is a heterohexamer, a central μ1 trimer with three σ3 monomers bound to its upper half. The N-terminal fragment of μ1 described above is largely buried within the base of the trimer, suggesting that major conformational changes must precede its release. There is ample evidence for structural transitions in the outer capsid, including conformational changes in μ1, which precede membrane perforation (Chandran et al., 2002, 2003; Odegard et al., 2004). The N-terminal eight residues (2–9) of μ1, as well as the myristoyl group attached to Gly2 (Nibert et al., 1991b; Tillotson and Shatkin, 1992), are not visible in the μ1-σ3 crystal structure, presumably because they were disordered in the crystals (Liemann et al., 2002) (Figure 1). A putative loop from residues 72–96 and the carboxyl (C)-terminal 33 residues (676–708) of μ1 were also apparently disordered in the crystals (Figure 1).

To learn more about the structure of μ1 in reovirus particles, we have turned to electron cryomicroscopy (cryo-EM) and three-dimensional (3D) image reconstruction. A series of previous cryo-EM reconstructions of virions, infectious subvirion particles (ISVPs), and recoated particles, all containing the μ1 protein or its fragments, have been determined at resolutions of 18 Å or lower (e.g., Chandran et al., 2001; Dryden et al., 1993; Liemann et al., 2002; Metcalf et al., 1991; Nason et al., 2001; Wilson et al., 2002). From these determinations, the virion outer capsid has been known to contain 200 μ1-σ3 heterohexamers assembled on an incomplete, fenestrated T = 13*l* lattice. Around each of the 12 icosahedral 5-fold axes, this lattice is substituted by pentamers of core-turret protein λ2, which mediates key functions in 5′-capping of the viral plus-strand RNA transcripts following entry into the cytoplasm (reviewed in Furuichi and Shatkin, 2000) and for which an X-ray crystal structure has been determined as part of the core particle (Reinisch et al., 2000). By fitting the X-ray models of μ1-σ3 and λ2 into an 18 Å cryo-EM map of the virion, we have previously derived an atomic model of the entire outer capsid (Liemann et al., 2002), missing only the fibrous cell adhesion protein σ1 and the small segments of μ1 described above.

Several groups have extended cryo-EM reconstructions of icosahedral virus particles to resolutions beyond 10 Å (reviewed in Henderson, 2004). Among these is our recently reported structure of the reovirus virion at ~7.6 Å resolution (Zhang et al., 2003). We have used this reconstruction to localize the viral RNA-dependent

*Correspondence: mnibert@hms.harvard.edu (M.L.N.); tsb@chem.ucsd.edu (T.S.B.)

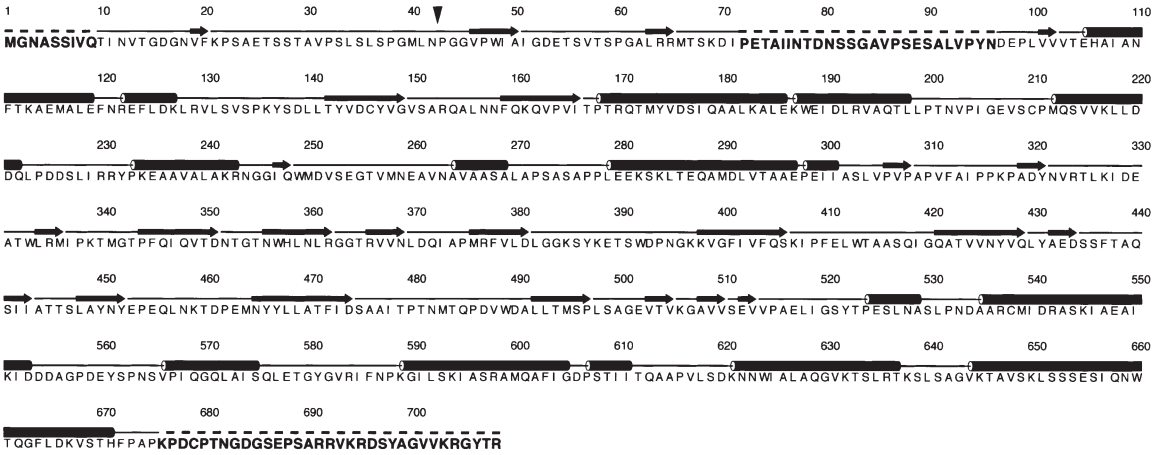

Figure 1. Sequence and Secondary Structures of Reovirus μ1 Protein

Primary sequence of reovirus μ1 protein (GenBank AAM10735) is shown in single-letter code with position numbers above. Three segments of disordered residues in the X-ray crystal model of the μ1-σ3 heterohexamer (Liemann et al., 2002) are indicated by larger, bold letters and dashed lines. Secondary structures extracted from the crystal structure are noted above the other sequences (α helices, cylinders; β strands, arrows). An arrowhead marks the autocleavage site between residues 42 and 43. The μ1 protein is N-terminally myristoylated, presumably on Gly2 after removal of Met1 (Nibert et al., 1991b; Tillotson and Shatkin, 1992).

RNA polymerase, λ3, a protein for which a crystal structure has also been determined (Tao et al., 2002). For the current study, we refined the cryo-EM reconstruction of the virion to ~7.0 Å resolution and used this structure to visualize several features of the outer capsid, including segments of μ1 that were disordered in the μ1-σ3 crystals. The newly visualized features appear to be important for stabilizing the outer capsid, regulating the conformational changes in μ1 that accompany perforation of target membranes, and contributing directly to membrane penetration during cell entry.

Results

Refined Cryo-EM Map of Reovirus Virion

We have estimated the mean resolution of our recent cryo-EM reconstruction of the virion of reovirus strain type 3 Dearing (T3D) to be 7.6 Å (Zhang et al., 2003). Further improvements in methods (see Experimental Procedures) permitted us to refine it to a mean resolution near 7.0 Å for the current report (Figures 2A and 3). Across most of the particle radii spanned by proteins λ1, λ2, σ2, and μ1 (240–396 Å) (Dryden et al., 1993), the estimated resolution of the refined map is slightly better, ranging between 7.0 Å and 6.7 Å (Figure 3 and data not shown).

Averaged Cryo-EM Map of Virion Bound μ1 Protein

For most types of icosahedral virus particles, each asymmetric unit contains more than one copy of the shell protein, and with standard icosahedral-reconstruction procedures, no additional symmetry operations are imposed to average the density among the different copies. After reconstruction, however, averaging the data for subunits adopting largely identical conformations within each asymmetric unit may improve the resolution of that part of the density map (Jiang et al., 2003; Zhou et al., 2000, 2001). The same holds for repeating subunits within nonicosahedral lattices, such as clathrin in hexagonal barrels (Fotin et al., 2004). Whether this method works to improve the resolution of any particular map can be determined only empirically, and we therefore addressed this possibility for virion bound μ1 in this study.

Although the reovirus outer capsid is organized with quasi T = 13*l* symmetry, only 10 of a possible 13 copies of μ1 are present per asymmetric unit, because a copy of λ2 occludes the other three positions (Dryden et al., 1993) (Figures 2B–2D). Nine of the ten μ1 subunits per asymmetric unit are contained in three uniquely positioned trimers, designated Q, R, and S; the tenth subunit is one-third of the T trimer, centered on the icosahedral 3-fold axis (Dryden et al., 1993) (Figures 2B–2D). After extracting data from the 7.0 Å cryo-EM map of the virion, we determined that the ten unique μ1 subunits have very similar conformations, as demonstrated by high correlation coefficients (0.89–0.96) in pairwise comparisons (data not shown). The coefficients were higher among subunits from the R, S, and T trimers (0.92–0.96), indicating that subunits from the Q trimer are less similar. We therefore omitted Q from the averaging procedure and used only the seven subunits from the R, S, and T trimers. The estimated mean resolution of the averaged map was improved to ~6.7 Å (Figure 3). Further improvement was likely limited by the accuracy of determinations of particle orientation and origin, as well as by the finite number of particle images used. A representative region showing improvements in the averaged μ1 map is illustrated in Figure 4. Despite its improved resolution, the averaged map revealed no significant additional features.

Comparisons of Cryo-EM Maps with X-Ray Models

We have previously described the fitting of X-ray crystal models of reovirus proteins into the 7.6 Å reconstruction of the reovirus T3D virion, and we focused on

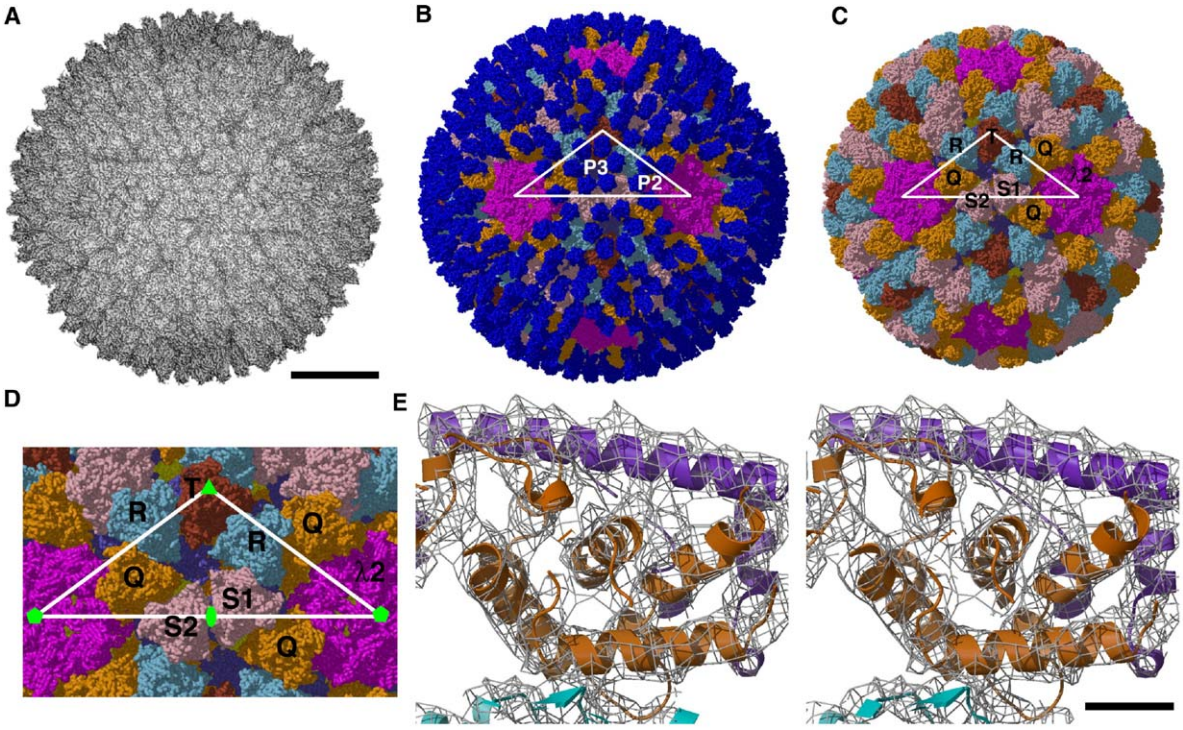

Figure 2. Cryo-EM Reconstruction of Reovirus Virion and Atomic Models of Virion and ISVP

(A) Shaded surface representation of 7.0 Å cryo-EM reconstruction of reovirus virion, viewed along an icosahedral 2-fold axis. The 200 Å scale bar also applies to (B) and (C) and represents 100 Å for (D).

(B) Atomic model of reovirus virion viewed as in (A). Proteins are differentiated by color: σ3 monomers, blue; λ2 pentamers, magenta; μ1.Q trimers, orange; μ1.R trimers, cyan; μ1.S trimers, pink; and μ1.T trimers, brown. The μ1 trimers are partially obscured by σ3 in the virion, but are clearly seen in the ISVP model in (C). P2 and P3 channels through the outer capsid are labeled; the former is bounded by four μ1 trimers and λ2, and the latter is bounded by six μ1 trimers (Dryden et al., 1993; Metcalf et al., 1991). One asymmetric unit, visible in this panel as well as in (C) and (D), is outlined with a white triangle.

(C) Same as shown in (B), but minus the σ3 subunits in order to model the ISVP. The different types of μ1 trimers that surround the P2 and P3 channels indicated in (B) are now labeled with letters. The two S trimers related by the icosahedral 2-fold axis are labeled S1 and S2 to signify that they have distinct interactions with the underlying σ2 monomer (not visible).

(D) Close-up view of a portion of the ISVP model shown in (C). Green symbols (pentagons, triangle, and oval) identify the icosahedral five-, three-, and 2-fold axes, respectively.

(E) Close-up stereo view of part of a μ1.T trimer. Cryo-EM densities attributable to μ1.T in the 7.0 Å map of the virion (gray net, contoured at 2.0 σ) have been fitted with a model of the μ1 trimer (ribbon traces colored in purple, orange, and cyan for the three respective subunits in this trimer) derived from the 2.8 Å X-ray crystal structure (Liemann et al., 2002). Scale bar, 10 Å.

core proteins λ1, λ2, λ3, and σ2 (Zhang et al., 2003). The fits showed strong correspondences between the X-ray models of λ1, λ2, and σ2 within core particles and their structures within the virion cryo-EM map, and they additionally allowed the position and orientation of λ3 within the virion to be determined. The fits also showed strong correspondences between the X-ray models of μ1 and σ3 within the μ1-σ3 heterohexamer (Liemann et al., 2002) and their structures at different lattice positions within the outer capsid region of the virion cryo-EM map. For the previous report, however, the outer capsid was not a focus of emphasis, and regions of μ1 missing from the X-ray model, but present in the cryo-EM map, were not examined.

For this report, we repeated fitting procedures for each of the indicated proteins by using the 7.0 Å map of the virion (e.g., Figure 2E) as well as the 6.7 Å map of the virion bound μ1 protein. In this manner, we made minor refinements to the previous results for the three core-surface proteins—λ1, λ2, and σ2—as well as for the position and orientation of the internal core protein and polymerase λ3 (data not shown). No crystal structure of the second internal core protein, μ2, is yet available for such analysis (Kim et al., 2004). We also refined the previous results for fitting the X-ray model of the μ1-σ3 heterohexamer into 200 positions in the outer capsid region of the 7.0 Å map of the virion (Figures 2B–2D). A number of findings about μ1 and its contacts with other proteins are discussed below. Findings for σ3 were essentially the same as those from the 7.6 Å map (Zhang et al., 2003): close correspondence between the X-ray model and the cryo-EM densities. Limited densities attributable to the base of the trimeric cell adhesion fiber σ1 (Chappell et al., 2002; Furlong et al., 1988) were observed in the 7.0 Å map, consistent with that protein's known flexibility. Since these densi-

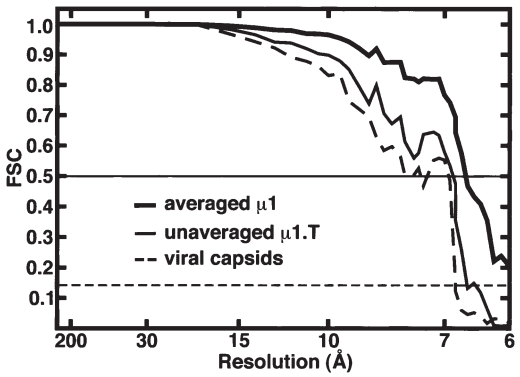

Figure 3. Resolutions of Virion and Averaged μ1 Subunit Maps

Plots of the Fourier-shell correlation (FSC) as a function of resolution are depicted for the virion capsids (dashed curve), the μ1.T trimer densities (solid curve), and the averaged μ1 subunit densities (thick solid curve). Based on a conservative threshold criterion (solid horizontal line for FSC = 0.5 [Rosenthal and Henderson, 2003]), the effective resolutions of the virion capsids, μ1.T trimer, and averaged μ1 subunit are approximately 7.0, 6.9, and 6.7 Å, respectively. Based on a less stringent, noise-limited criterion (dashed horizontal line for FSC = 0.143 [Rosenthal and Henderson, 2003]), the effective resolutions are approximately 6.8, 6.7, and better than 6.0 Å, respectively. The FSC for the μ1 average exceeds that for the other two density maps at all resolutions, indicating that all features ≥ 6.0 Å are better represented in the average.

ties were similar to ones in previous reconstructions of reovirus particles (e.g., Chandran et al., 2001; Dryden et al., 1993, 1998; Liemann et al., 2002; Wilson et al., 2002), they were not analyzed further for this report.

Discussion

Positions of the C-Terminal Arm of Outer Capsid Protein μ1

Several previous cryo-EM reconstructions of reovirus virions and recoated cores (Chandran et al., 1999, 2001; Dryden et al., 1993, 1998; Liemann et al., 2002; Nason et al., 2001), at resolutions lower than reported here, revealed a disconnected density, or "blob," in each of the P3 channels through the outer capsid (see Figure 2 for terminology). The particle radii at which these blobs were found suggested that they might be attributable to the 33 C-terminal residues (676–708) of μ1, which were disordered in the μ1-σ3 crystals (Liemann et al., 2002).

In the 7.0 Å reconstruction of the virion, more details of these features are now visible. Especially notable are six "spokes" (~10 Å long × ~7 Å wide) connecting the central "hub" of each structure to the bodies of the six surrounding μ1 trimers (Figure 5A). Each spoke connects to the associated μ1 subunit near the last residue of the fitted X-ray crystal model of μ1, Pro675 (Figures 5A and 5B). The spokes run from this position in a slightly inward radial direction before connecting to the hub (Figure 5B). The hub resembles a squat cylinder (~26 Å tall × ~20 Å wide), possibly pierced by a small radial channel (Figure 5A).

The top-most parts of the hub appear to be more ragged and have lower density values than the bottom (Figure 5B), suggesting that the top may include more flexible elements. The spokes also have lower density values than the bulk of μ1, suggesting that they too are more flexible. When the density-contour level is raised from 0.5 to 1.5 σ, the total volume of one P3 hub-and-spokes structure goes from accounting for ~22 residues per subunit to completely disappearing, even though most other features of μ1 show only minor changes. These results not only suggest a higher level of flexibility in this region but also indicate that some of the C-terminal 33 residues of μ1 that are missing from the X-ray model may still not be fully represented in the virion map.

A related structure is also found in each P2 channel. The P2 structures differ in having only four spokes (Figure 5C), consistent with the presence of only four μ1 trimers around each of these channels (Dryden et al., 1993; Liemann et al., 2002). The central hub of the P2 complex resembles a squat cylinder that is flattened on one side (Figure 5D), consistent with the fact that the two μ1 trimers that fill that side of the cylinder in each P3 channel are missing, substituted by λ2. Thus, the motif that constitutes the hub may fold into a similar, but incomplete, structure with contributions from only four μ1 subunits. Overall, the hub and spokes in each P2 channel have lower density values than those in each P3 channel, suggesting that the P2 structures are even more flexible.

By tying together the C termini of four or six μ1 subunits, the hub-and-spokes complexes may be critical for assembling or stabilizing the entire μ1 lattice. The structures may also contact core proteins λ2 and/or σ2 (Figures 5C and 5D). Recoating experiments have shown that deletion of nine C-terminal residues (700–708) of μ1 does not prevent assembly of the outer capsid, but deletion of 22 residues (687–708) does (A.L. Odegard and M.L.N., unpublished data). Thus, some portion of the hub-and-spokes complex is probably required for stable assembly of the μ1 layer. The C-terminal sequences of μ1 are not represented in the μ1 homologs of avian orthoreoviruses (Noad et al., 2005) or aquareoviruses (Attoui et al., 2002), suggesting that these residues do not have a conserved, essential role.

The length of each spoke (~10 Å) in the P2 and P3 structures would seem to place residue Cys679 near the junction with the central hub. This is consistent with the capacity of Cys679 to form disulfide bonds between pairs of subunits in the maturing outer capsid (Odegard et al., 2003). Sequences following Cys679 in all four or six subunits then presumably coalesce to form the hub. The Cys679-mediated disulfide bonds may help to stabilize the complex, but they are probably not the sole features that tie together the C termini of the surrounding subunits. Indeed, a mutant μ1 in which Cys679 has been substituted by serine is fully competent for outer capsid assembly and generation of infectious virion-like particles by recoating (Odegard et al., 2003).

Evidence that the C-terminal 14 residues (695–708) of μ1 in virions are sensitive to protease cleavage and release (Mendez et al., 2003; Nibert, 1993) favors the idea that these sequences extend from the top of the hub. After these residues are removed by proteolysis during generation of ISVPs, the hub-and-spokes complexes remain visible in a 12 Å cryo-EM reconstruction

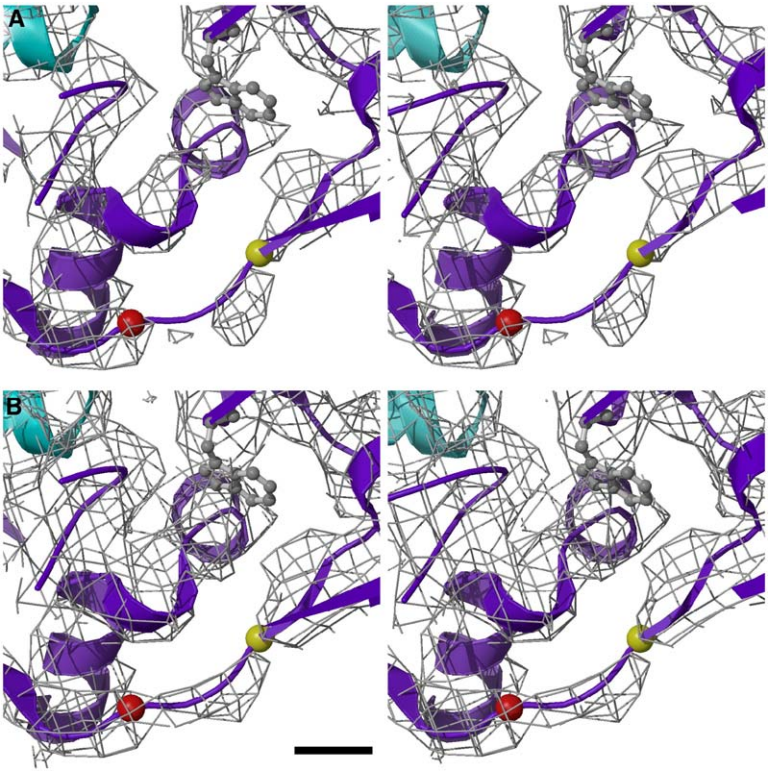

Figure 4. Cryo-EM Densities of μ1 before and after Averaging

(A) Close-up stereo view of a portion of the μ1.T trimer before nonicosahedral averaging of the cryo-EM densities. The densities (gray net, contoured at 2.0 σ) have been fitted with the X-ray crystal model of the μ1 trimer (purple and cyan ribbon traces for two respective μ1 subunits from the same trimer). At this contour level, densities attributable to residues Pro316–Ala319 (red and yellow spheres, respectively, connected by purple trace) are discontinuous, and there is little density attributable to the side chain of Trp333 (ball and stick model).

(B) Same as shown in (A), but for the nonicosahedral average of seven μ1 subunits (see Experimental Procedures). At a contour level of 2.0 σ, the cryo-EM densities attributable to residues Pro316–Ala319 are now nearly continuous, and there is somewhat more density attributable to the side chain of Trp333 (the latter being more evident when viewed from a different angle than the one chosen to highlight the 316–319 region in this figure). The 5 Å scale bar also applies to (A).

(X.Z., M.A. Agosto, M.L.N., and T.S.B., unpublished data). Thus, these C-terminal sequences are not required for structural integrity of the μ1 layer or infectivity of the ISVP. Removal of these sequences in fact might be necessary for μ1 to function in cell entry (Mendez et al., 2003).

Positions of the 72–96 Loop of μ1

In the X-ray crystal model of μ1-σ3 (Liemann et al., 2002), Ile71 and Asp97 are exposed on the heterohexamer surface, near the base of each μ1 subunit at radii 300 Å and 308 Å, respectively (Figure 6). These locations suggest that the intervening loop, disordered in the crystals, might project either sideways toward an adjacent μ1 or λ2 subunit or inward toward a σ2 or λ1 subunit in the virion.

In the 7.0 Å cryo-EM map of the virion, densities attributable to residues 72–96 are visible, adjoining the body of μ1 where residues 71 and 97 are exposed (Figure 6). For nine of the ten μ1 subunits (all but one of the Q subunits) in each asymmetric unit, the features of the loop densities are as follows. The loop projects largely sideways, toward an adjacent μ1 trimer, and its volume can account for most of the 25 loop residues. The loop appears to contact two different subunits in the adjacent trimer: across the C-terminal end of a short α helix (helix, 122–127; contacts, between 126 and 129) in one subunit and with the C-terminal part of a loop and the succeeding β strand (loop, 51–62; strand, 63–65; contacts, between 57 and 65) in another (Figure 6). The 122–127 α helix from the X-ray model, when fitted into the cryo-EM densities, appears to be slightly displaced, perhaps because of the loop contacts that are unique to particle bound μ1 (see next paragraph). In addition, densities attributed to the 72–96 loop appear to connect with other newly visualized densities attributed to the N-terminal arm of the same opposing subunit as contributes the 126–129 contacts (see later section and Figures 8C and 8D). Densities attributable to this loop are also visible, although less well defined, in the 12 Å cryo-EM map of the ISVP (X.Z. et al., unpublished data). The loop is not seen in the μ1-σ3 crystal structure (Liemann et al., 2002), evidently because contacts with the adjacent μ1 trimer in the particle are required for maintaining an ordered structure.

For the one μ1.Q subunit in each asymmetric unit for which the 72–96 loop abuts λ2, the loop remains poorly defined (data not shown). Only limited new density is seen adjoining residue 97 and projecting toward λ2. Even when a lower density contour level is used for displaying the map, only a few additional beads of density are visible to suggest the loop's path. We conclude that the loop makes only weak contacts with λ2. In the one Q subunit for which the 122–127 α helix abuts λ2 and therefore does not contact the 72–96 loop from an adjacent μ1 trimer, the helix does not appear to be displaced and instead contacts the 580–586 loop from λ2 (see later section and Figures 8C and 8D).

The trimer-trimer contacts by the 72–96 loop probably help to stabilize the μ1 lattice in both virions and ISVPs. In addition, the loop may stabilize the base of the adjacent trimer, by making contacts with two different subunits within that trimer. These contacts by the 72–96 loop would likely need to break during the con-

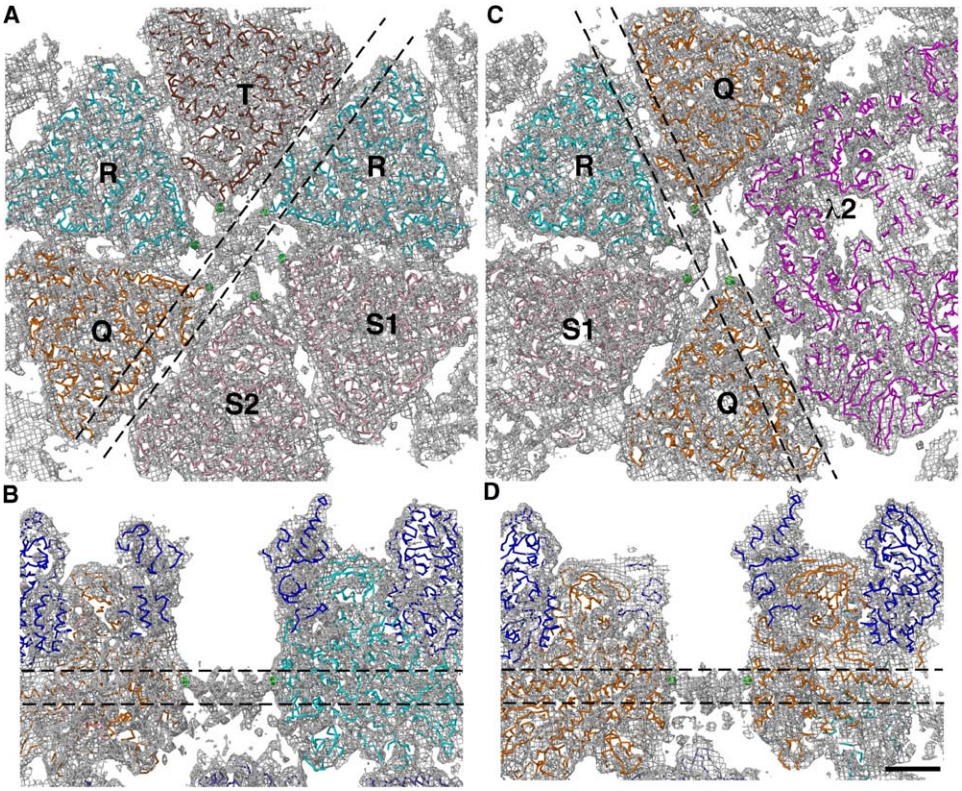

Figure 5. Cryo-EM Densities in the P3 and P2 Channels of Reovirus Virion

(A–D) Cryo-EM densities (gray net) are contoured at 0.8 σ. Colors and labels correspond to those in Figures 2B–2D. Ribbon traces depict the fitted X-ray crystal models of the (A–D) μ1 trimers (Q, orange; R, cyan; S, pink, and T, brown), (B and D) associated σ3 monomers (blue), a (C and D) λ2 pentamer (magenta), and (B and D) σ2 monomers (purple). Pro675, the last residue visible in the μ1 crystal structure, is identified with a green ball for the μ1 subunits that project it into the highlighted (A and B) P3 and (C and D) P2 channels. "Hub-and-spokes" cryo-EM densities, devoid of fitted models but abutting Pro675, are visible in the channels, with six spokes in the P3 structure and four spokes in the P2 structure. (A) The slab shown in this panel is from the region bounded by dashed lines in (B). A radial channel through the P3 hub is more evident at lower resolutions (8–9 Å). (B) P3 channel, side view. The slab is from the region bounded by dashed lines in (A). (C) P2 channel, top view. The slab is from the region bounded by dashed lines in (D). (D) P2 channel, side view. The slab is from the region bounded by dashed lines in (C). The 25 Å scale bar applies to all panels.

formational changes in μ1 that accompany cell entry (Chandran et al., 2002, 2003; Odegard et al., 2004).

Shifts in the 51–62 Loop of μ1

A loop that spans μ1 residues 51–62 in the X-ray crystal model of μ1-σ3 (Liemann et al., 2002) "hangs" from the base of each subunit (Figure 6C). Densities attributable to each of these loops in the virion cryo-EM map are, in nine of the ten μ1 subunits, displaced from their positions in the crystal structure. The only subunit in which the 51–62 loop is not substantially shifted is the one λ2-contacting subunit in each Q trimer that also contacts the σ2.5f nodule (see later section for terminology) (data not shown). In addition, in most of the other subunits, a middle portion of the 51–62 loop shows thinned or absent density in the cryo-EM map (Figure 6C and data not shown). The reasons for these shifts in the 51–62 loop are not obvious, but they could result in part from contacts with the ordered 72–96 loop that projects from the μ1 subunit on the opposite side of the 2-fold or quasi-2-fold axis and appears to have "pulled" the 51–62 loop up and to one side (Figure 6C). For some μ1 subunits, additional contacts with an underlying σ2 subunit may help to determine the precise conformation of the 51–62 loop (data not shown). Thus, the 51–62 loop may participate in stabilizing the μ1 lattice as well as in anchoring this lattice to the underlying inner capsid.

Structure around the Autocatalytic Cleavage Site of μ1

The 708 residue μ1 protein undergoes an autocatalytic cleavage (autocleavage) between residues Asn42 and Pro43, yielding myristoylated N-terminal fragment μ1N and C-terminal fragment μ1C (Nibert et al., 1991b, 2005; Smith et al., 1969). If this cleavage cannot occur, the particles are minimally infectious, possibly because the μ1N peptide cannot be released during cell entry (Odegard et al., 2004). The μ1N/μ1C cleavage has been thought to occur before or during assembly, when σ3 associates with μ1 to form the μ1-σ3 heterohexamers, which then go on to form the outer capsid (Chandran et al., 1999; Lee et al., 1981; Shing and Coombs, 1996). Recent results involving changes to the conditions for

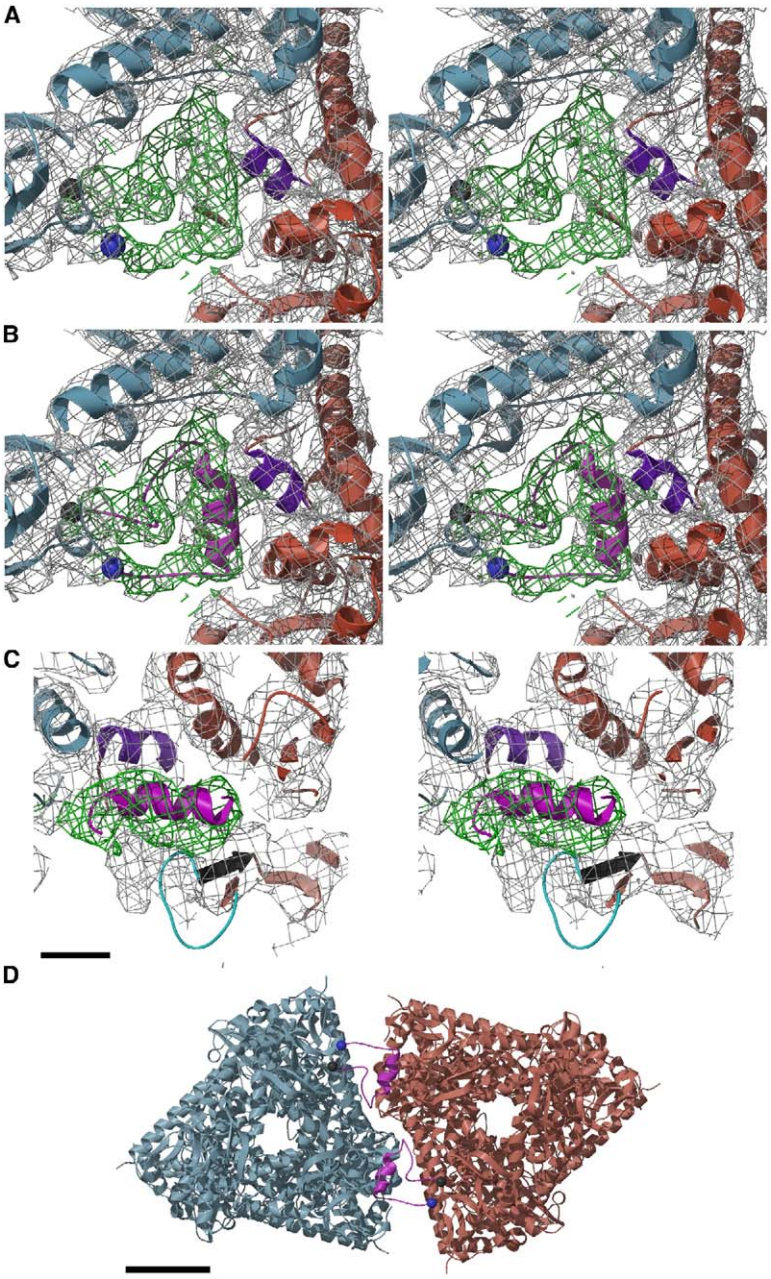

Figure 6. Cryo-EM Densities for Residues 72–96 in the Averaged μ1 Cryo-EM Map

(A) Close-up stereo view of a region near the base of two adjacent μ1 trimers, looking toward the virion interior. Cryo-EM densities (gray net, contoured at 2.0 σ) are fitted with the X-ray crystal models of two μ1 trimers (light-blue and brown ribbon traces, respectively). Extra cryo-EM densities forming a U-shaped loop (green net) were assigned to residues 72–96. Black and blue spheres, abutting the two ends of the U-shaped densities, identify the positions of residues Ile71 and Asp97, respectively, in the light-blue subunit. A short α helix (residues 122–127), colored purple in the otherwise brown subunit, is slightly displaced from the attributed cryo-EM densities, apparently owing to contacts with the 72–96 loop.

(B) Same as shown in (A), but with a tentative ribbon trace (magenta), including an α helix, built into the extra cryo-EM densities ascribed to residues 72–96.

(C) Same as shown in (B), but viewed in an orthogonal direction, from the left side of (B) to illustrate apparent interactions between the 72–96 (magenta) and the 51–62 (cyan) loops. The 51–62 loop is clearly displaced from the associated cryo-EM densities. A β strand formed by residues 63–65 (black) also contacts the 72–96 loop. The 10 Å scale bar also applies to (A) and (B).

(D) Bottom view (from virion interior) of two adjacent μ1 trimers (light-blue and brown) in the atomic model. Putative traces for the two 72–96 loops at the trimer-trimer interface are shown in magenta. The scale bar is 25 Å.

particle disruption before electrophoresis indicate, however, that many more of the μ1 subunits than previously thought remain uncleaved in virions and ISVPs and undergo this cleavage only later, in concert with outer capsid disassembly (Nibert et al., 2005). The μ1-σ3 crystal structure nonetheless reveals a cleaved form of μ1, in which the peptide bond between Asn42 and Pro43 has been broken and the two termini have moved ~9 Å apart (Liemann et al., 2002) (Figure 7).

Comparing the cryo-EM map of μ1 in virions with the X-ray crystal model of μ1-σ3, we find that the region around the autocleavage site exhibits a few key differences (Figure 7). Residues from the X-ray model leading up to and including Asn42 fit well with densities in the cryo-EM map, but Pro43 and Gly44 from the crystal structure are displaced. Moreover, density from Asn42 through to Gly45 in the cryo-EM map appears to form a continuous bridge, which persists over a wide range of density contour levels. Similar densities are evident for μ1 subunits in each of the ten positions in the asymmetric unit. We conclude that the Asn42/Pro43 peptide bond remains uncleaved in many of the virion bound subunits. The resolution of the cryo-EM map is not high enough for this conclusion to be definitive, and because the map is an average, we cannot conclude that this bond remains uncleaved in all subunits. The conclusion is nonetheless consistent with the recent biochemical findings (Nibert et al., 2005) and supports the hypothesis put forth in Nibert et al.'s study that many of the μ1 subunits in virions remain uncleaved at the

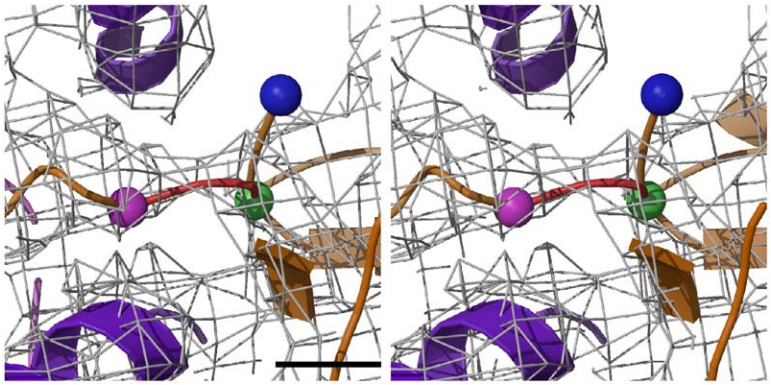

Figure 7. Autocleavage Site in the Averaged μ1 Cryo-EM Map

Portions of two μ1 subunits from the same trimer (indicated by purple and orange traces for the X-ray crystal models of these subunits) are shown in a close-up stereo view. The positions of Asn42, Pro43, and Gly45, as found in the cleaved μ1 subunits of crystallized μ1-σ3 heterohexamers (Liemann et al., 2002), are indicated with magenta, blue, and green spheres, respectively. Asn42 lies within the cryo-EM densities (gray net, contoured at 1.8 σ), whereas Pro43 and Gly44 (no sphere) lie outside, and these observations hold true over a broad range of contour levels (data not shown). Furthermore, unlike in the X-ray crystal structure, a continuous arch of density bridges residues 42–45 in the cryo-EM map, suggesting that the Asn42/Pro43 peptide bond remains uncleaved. The red trace within this arch models the putative path of μ1 residues 42–45 within the virion. The scale bar is 5 Å.

μ1N/μ1C junction until outer capsid disassembly. The μ1-σ3 crystal structure may contain μ1 in the cleaved form because the autocleavage was induced during crystallization (Liemann et al., 2002).

Positions of the N-Terminal Arm and Myristoyl Group of μ1

In the μ1-σ3 crystal structure (Liemann et al., 2002), Thr10 is the first visible residue and is exposed on the heterohexamer surface, near the base of each μ1 subunit at radius 316 Å (Figure 8A). Approximately 17 Å above Thr10, on the same side of μ1, is the opening to a narrow hydrophobic pocket that extends into the μ1 interior. This pocket is deep enough to accommodate a myristoyl chain, but in the crystal structure it is occupied instead by β-octylglucoside, a detergent from the buffer. It was proposed that the myristoyl group would occupy this pocket in the absence of detergent and that residues 2–9 could readily link it to the position of Thr10.

In the 7.0 Å cryo-EM reconstruction of the virion, new densities are seen that are consistent with this proposal, forming an arc that links Thr10 to the putative myristoyl binding pocket (Figure 8). Similar densities are evident for μ1 subunits in each of the ten unique positions in the outer capsid, including the one Q subunit in which this region abuts λ2. Because these features are weaker than those for the 72–96 loop, our conclusions about them are more tentative. Nevertheless, we conclude from the observations that the locations of the missing N-terminal regions of μ1 proposed by Liemann et al. (2002) are probably correct. The weaker density suggests that this region is reasonably flexible, and it remains possible that the myristoyl group may move in and out of the hydrophobic pocket as the structure "breathes."

The N-terminal region of the μ1.Q subunit that contacts λ2 appears to affect the position of the 580–586 loop of λ2, as revealed by displacement of the assigned cryo-EM densities from the position of this loop in the X-ray model of the core particle (Reinisch et al., 2000) (Figure 8C). The 580–586 loop of λ2 additionally contacts α helix 122–127 of the μ1.Q subunit (Figure 8C; also described above) and possibly mediates ionic interactions between Asp583 and Asp586 of λ2 and Lys127 and Arg129 of μ1. The 580–586 loop belongs to the methylase-1 domain of λ2 and contains residues that also change position upon binding of the methyl-donor substrate, *S*-adenosyl-L-methionine (Reinisch et al., 2000). The interactions with μ1.Q could conceivably inhibit the λ2 methylase-1 by freezing the conformation of the substrate binding pocket.

The N-terminal region of μ1 appears to have a role in cell entry (Nibert et al., 1991b; Odegard et al., 2004). Even if fully extended, the length of a myristoyl group and eight amino acid residues of μ1 (2–9) would be about 48 Å, much less than needed to reach above the outermost surface of μ1 (radius 396 Å) in virions and ISVPs. Thus, the myristoyl group would not be accessible to the cellular membrane unless conformational changes in μ1 released it to move or even to dissociate from the particle as part of the autolytically released μ1N peptide (Odegard et al., 2004).

The densities we assign to the N terminus of μ1 merge with the 72–96 loop densities that reach across from the adjacent μ1 trimer. Thus, some residues within this N-terminal region, most likely Ile7–Gln9 may contribute contacts that stabilize the 2-fold interactions between μ1 trimers. This is the part of the N-terminal region for which assigned densities are strongest, perhaps because the loop contacts make them less flexible. These are additional contacts that would need to break in order for the myristoylated μ1N peptide to be released in association with cell entry.

Other Contacts among μ1 Trimers, and between μ1 Trimers and Core Proteins

In addition to contacts mediated by the N- and C-terminal extensions and the 51–62 and 72–96 loops described above, the bodies of the μ1 trimers engage in other contacts. These contacts were previously suggested, but not extensively described, by Liemann et al. (2002). The 7.0 Å cryo-EM reconstruction of the virion further delimits these contacts.

The four types of μ1 trimers in an asymmetric unit engage one another in side-to-side contacts across five different types of 2-fold (S-S) or quasi-2-fold (Q-R, Q-S, R-S, and R-T) interfaces (see Figures 2C and 2D). Trimer-trimer contacts are concentrated in two regions of each of these interfaces, one near the top, centered

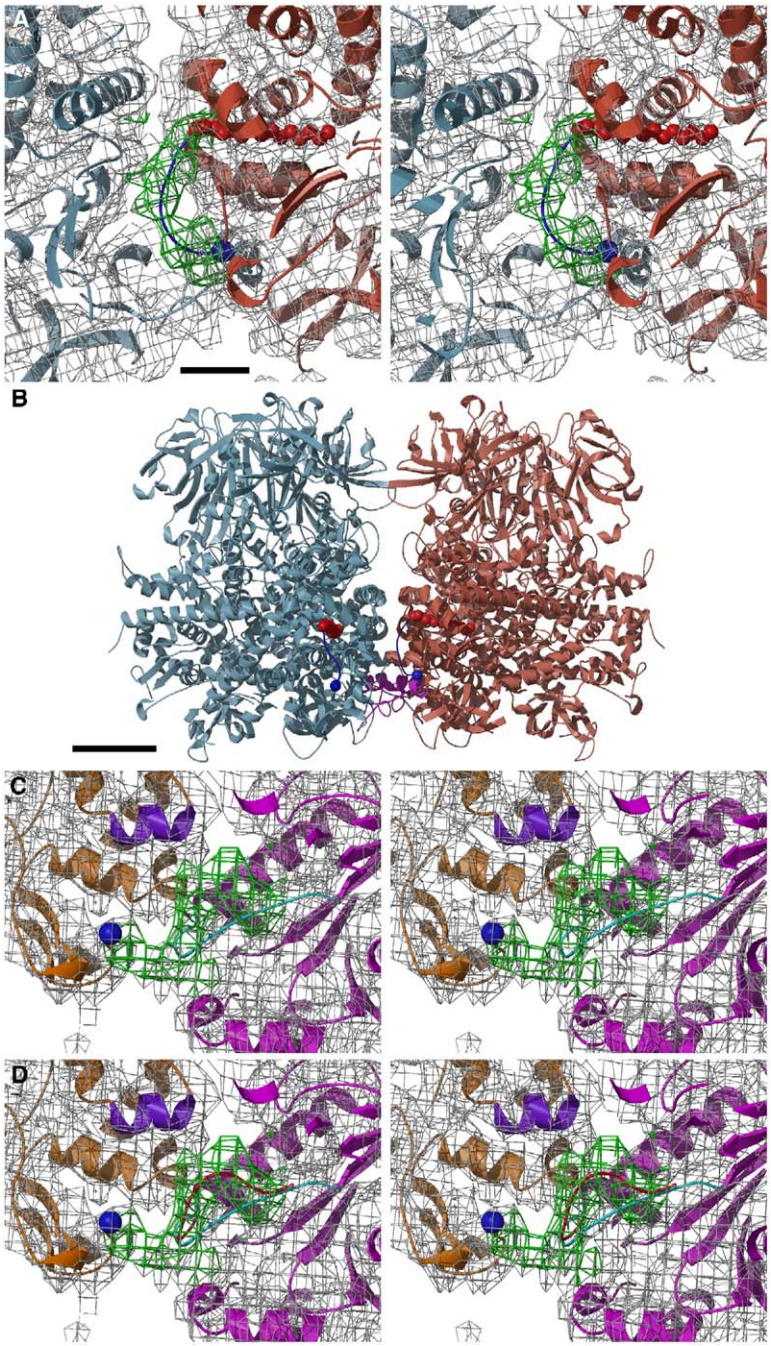

Figure 8. Cryo-EM Densities for N-Terminal Eight Residues of μ1 and Residues 580–586 of λ2

(A) Close-up stereoview of the cryoEM densities (gray net) and fitted X-ray crystal models (light-blue and brown ribbon traces) at the interface between two μ1 trimers. Extra cryo-EM densities (green net) have been assigned to the N-terminal eight residues of one μ1 subunit from the orange trimer. The position of Thr10 is marked by a blue sphere, residues Gly2 to Gln9 are modeled as a blue loop, and the N-terminal myristoyl group is represented as a space-filling model (red) occupying the β-octylglucoside pocket. Densities shown here, for the averaged μ1 subunits, are contoured at 1.4 σ. The 10 Å scale bar also applies to (C) and (D).

(B) Same as shown in Figure 6D, but viewed in an orthogonal direction (from the bottom of Figure 6D) to show a full side view of the pair of μ1 trimers. Also highlighted are the putative trace for N-terminal residues 2–9 (blue) and the space-filling model for the N-terminal myristoyl group (red), for the one subunit in each trimer for which this region is positioned near the highlighted trimer-trimer interface. The scale bar is 25 Å.

(C) Close-up view of the 7.0 Å virion reconstruction showing cryo-EM densities (gray net, contoured at 1.6 σ) and fitted X-ray models (ribbon traces) at the interface between the μ1.Q trimer (orange) and λ2 (magenta). Extra cryo-EM densities (green net) have been assigned to the 580–586 loop (cyan trace) of the λ2 methylase-1 domain and to approximately two residues of the N terminus of μ1 (blue sphere marks the position of Thr10). The short, purple-colored α helix in μ1 (residues 122–127) contacts the upper surface of the 580–586 loop of λ2. Conformation of the λ2 loop in the X-ray model of the core particle (Reinisch et al., 2000) places the loop outside the extra density, which indicates that interactions of λ2 with the neighboring μ1 subunit in virions results in a new loop conformation.

(D) Same as shown in (C), but with a putative model (red trace) showing a proposed conformation of the 580–586 loop of λ2 fitted into the extra cryo-EM densities.

at radius 375 Å, and the other near the base, centered at 320 Å (Figures 9A and 9B). The new atomic model derived from fitting the X-ray crystal model of μ1-σ3 into the 7.0 Å cryo-EM map of the virion suggests that each of these interfaces involves mostly the same contacting residues from the opposite sides, although there are minor differences reflecting either quasiequivalence or deficiencies in the model (data not shown). Most of the contacting residues are polar and contribute roughly 1350 Å^2 of buried surface per side of each interface.

Each μ1.Q trimer is engaged in additional side-to-side contacts with two adjacent λ2 subunits (Figure 9C). These λ2 contacts are extensive, contributing about 1900 Å^2 of buried surface on each Q trimer, and thus may play an important role in anchoring the μ1 layer to the core. Several of the residues that contact λ2 from the side of the Q trimer are the same ones (in terms of primary sequence position) that contact an adjacent μ1 trimer at other positions in the outer capsid (Figure 9C). In addition, according to the atomic model, a number of other, mostly polar residues in the μ1.Q subunits are uniquely engaged in λ2 contacts (Figure 9C). The "top" domain (Liemann et al., 2002) of the Q

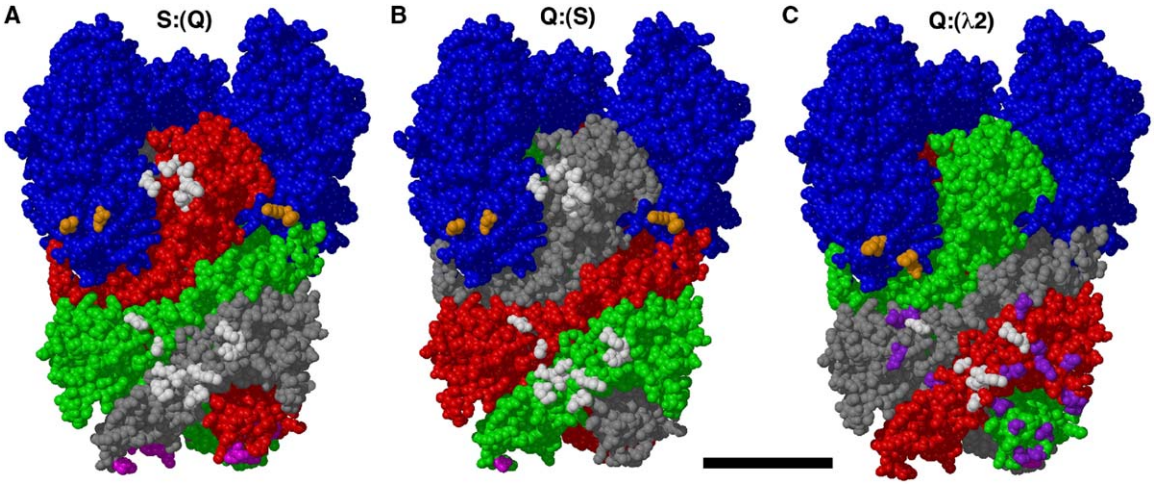

Figure 9. Contacts between μ1-σ3 Heterohexamers and between the μ1-σ3 Heterohexamer and λ2 Pentamer

(A) Space-filling model of the μ1-σ3.S heterohexamer viewed from the direction of the surface that contacts a μ1-σ3.Q heterohexamer. Three σ3 subunits (blue) sit atop the intertwined red, green, and gray μ1 subunits in the S heterohexamer. White highlights those residues in μ1 and σ3 that contact μ1 subunits in the Q heterohexamer. Orange highlights those residues in σ3 that contact σ3 subunits in the Q heterohexamer. Magenta highlights those residues at the bottom of μ1 that contact σ2 subunits in the core (not shown).

(B) Same as shown in (A), but for a view of the μ1-σ3.Q heterohexamer surface that contacts the μ1-σ3.S heterohexamer. The color scheme is identical to that in (A).

(C) Same as shown in (B), but for a view of the μ1-σ3.Q heterohexamer surface that contacts the λ2 pentamer. White and purple highlight those residues in μ1 that contact λ2; white highlights residues that, on the other two faces of the Q heterohexamer, contact μ1 subunits in the R and S heterohexamers, whereas purple highlights residues that uniquely contact λ2. The remaining color scheme is the same as in (A). The 50 Å scale bar applies to all panels.

trimer has no contacts with λ2, which means that in one of its subunits, a side of the top domain covered by contacts with an adjacent μ1 subunit at other positions is uniquely exposed to solution. On the side of λ2, the contacts with μ1.Q involve residues in the guanylyltransferase domain, the so-called scaffold or bridge domain (Liemann et al., 2002; Reinisch et al., 2000), and the C-terminal methyltransferase (methylase-2) domain of one λ2 subunit and the N-terminal methyltransferase (methylase-1) domain of a neighboring λ2 subunit (data not shown).

The 200 μ1 trimers sit atop 150 monomeric σ2 nodules that decorate the core surface. The σ2 subunits comprise three types: 60 surrounding the λ2 pentamers (σ2.5f), 60 surrounding the icosahedral 3-fold axes (σ2.3f), and 30 crossing the icosahedral 2-fold axes (σ2.2f) (Reinisch et al., 2000). All contacts between μ1 and σ2 occur across a narrow range of particle radii, 292–301 Å, and involve the bottom surface of μ1 and the top surface of σ2 (Liemann et al., 2002; Reinisch et al., 2000). Each μ1 trimer contacts between one and three σ2 nodules, and the buried surface per side of these different interfaces varies from as little as 200 Å^2 to as large as 1650 Å^2. With regard to these contacts, there are five different types of μ1 trimers: Q, R, T, and two different types of S trimers (see Figure 2C). One subunit in each Q trimer (one of the same subunits as contacts λ2) weakly contacts a σ2.5f monomer; two subunits in each R trimer, respectively, contact a σ2.5f and a σ2.3f monomer; the three subunits in each T trimer make identical contacts with the three σ2.3f monomers around each 3-fold axis; and two subunits in each S trimer, respectively, contact a σ2.2f and a σ2.5f nodule (data not shown). The two different types of S trimer are based on the fact that either end of a single σ2.2f monomer contacts a different S trimer on either side of the icosahedral 2-fold axis (Reinisch et al., 2000). The flexibility of the 51–62 loops that "hang" from the base of each μ1 trimer (see Figure 6C) appears to be important for optimizing contacts with the different σ2 subunits that are made by that region in the Q, R, and S trimers. However, in the R and S trimers, a number of residues outside the 51–62 loops also contact σ2. The σ2 contacts made by the T trimers do not involve these loops. As at the μ1 trimer-trimer and μ1-λ2 interfaces, most of the contacting residues at the μ1-σ2 interfaces are polar. The set of residues in σ2 that is contacted by each type of μ1 trimer is largely distinctive.

Conclusions

The results of this study extend our model of the reovirus outer capsid and suggest new hypotheses about the mechanisms of outer capsid assembly and stability and the roles of μ1 in cell entry. Each μ1 trimer participates in multiple contacts with adjacent μ1 trimers and σ2 subunits, as well as with λ2 subunits in the case of the μ1.Q trimer, which not only stabilize the outer capsid but also constrain the conformational rearrangements that accompany cell entry. The high activation energy associated with these rearrangements (Middleton et al., 2002) is consistent with there being such a large number of broken contacts. By altering these intersubunit interactions through selective mutation of specific residues in μ1 or the other proteins, we should

gain a better understanding of how and where the conformational changes are initiated and propagated.

A remaining question is how the virion- and ISVP-associated μ1 layer inhibits mRNA synthesis by those particles (Chandran et al., 1999; Farsetta et al., 2000; Luongo et al., 2002), despite the fact that λ1, λ2, and σ2 intervene between μ1 and the internal transcriptase components λ3 (the RdRp) and μ2 (Dryden et al., 1998; Zhang et al., 2003). Considering that μ1 contacts only λ2 and σ2 within the core, the question is then how μ1 transmits signals to the transcriptase complex first through one or both of those proteins, and then through the λ1 shell. We hypothesize that μ1 represses the transcriptase complex through a series of signal-transducing interactions among the core proteins, with structural displacements of only a few Å—beyond the resolution of current results—providing the major effects.

Experimental Procedures

Purified Virions

Reovirus T3D virions were grown in spinner-adapted mouse L929 cells and purified from sonicated cell lysates by extraction with trichlorotrifluoroethane (Fisher) and equilibrium ultracentrifugation in CsCl (ICN Biomedicals) density gradients according to standard procedures (Furlong et al., 1988). The virus stock was one originally obtained from B.N. Fields.

Refinement of Reovirus Virion Reconstruction beyond 7.6 Å Resolution

A reconstruction of the reovirus T3D virion at 7.6 Å resolution and the same set of particle images as used to compute it (Zhang et al., 2003) were newly used to initiate refinement at higher resolutions, and no images were eliminated during the course of this procedure. For refining particle orientations and origins, we developed a new model-based parallel algorithm that is less sensitive to noise caused by experimental errors than are the algorithms used previously. The new algorithm, which has an added benefit of accommodating analysis of particles of any symmetry, has been implemented in the program PO^{2}R (Parallel Orientation and Origin Refinement), written in C and FORTRAN (Ji et al., 2005). Briefly, this program computes a two-dimensional (2D) discrete Fourier transform (DFT) of each particle image, applies a correction for the effects of the microscope contrast-transfer function, and compares the corrected 2D DFT with a series of neighboring central sections of the 3D DFT of the particle reconstruction. The central sections were chosen such that their orientations spanned our best current estimate of the particle's orientation. A "discrepancy distance" metric was used to define how well the 2D DFT of an image correlated with each calculated section of the 3D DFT. Hence, the central section that most closely matched the 2D DFT of the experimental image specified the refined orientation. Each cycle of refinement began with a coarse (1°) search of all three angles that define the orientation and centered about the current best estimate of the orientation. This was followed by finer (0.1°) and finer (0.01°) search intervals, with each search centered about the more precise orientation obtained in the preceding step. At the end of each cycle of orientation refinement, the centers of the particle images were similarly refined, with step sizes ranging from 1 to 0.01 pixels (2.2–0.022 Å in the specimen). A total of ~100 cycles of orientation/origin refinement was used to extend the resolution of the virion reconstruction from the previous 7.6 Å to the current 7.0 Å.

For computing the 3D reconstruction from the selected particle images, we have developed a family of parallel algorithms that operate within a Cartesian rather than a cylindrical coordinate system. As a result, Fourier coefficients of the 3D DFT are determined at the points of a cubic lattice (Lynch et al., 1999), and molecules of any symmetry can be handled in a straightforward manner (Marinescu et al., 2001). The algorithms, implemented in the program P3DR (Parallel 3D Reconstruction), comprise several stages of computation including initialization, 2D Fourier analysis, estimating the 3D coefficients of the DFT by interpolation, contrast transfer function correction, and 3D Fourier synthesis. The final virion reconstruction was computed to a resolution limit of 6.5 Å, by using an inverse temperature factor of 1/400 Å^2 to enhance the high-resolution features out to 7.0 Å (Havelka et al., 1995), after which the inverse factor was held constant and a Gaussian function was applied to smoothly attenuate the Fourier data to zero from 7.0–6.5 Å.

The PO^{2}R and P3DR programs were designed for clusters of workstations and parallel computers. For this study, the programs were run on a 44-node Linux PC cluster with each node consisting of two 2.4-GHz Pentium 4 processors and a shared memory of 3 GB (132 GB in total). Each cycle of refinement required ~14 hr.

Resolution decreased across the higher particle radii spanned by surface protein σ3 (data not shown), possibly because, at progressively higher radii, σ3 is embedded in a higher proportion of solvent, which contributes mainly noise to the reconstructed map. The upper parts of σ3 may also have greater flexibility, which would further decrease their resolution in the map. Resolution also decreased across the lower radii spanned by the viral RdRp λ3 (Tao et al., 2002; Zhang et al., 2003) and the dsRNA genome segments (data not shown), most likely due to the increasing fraction of non-icosahedrally ordered density contributed by the genome at progressively lower radii. Moreover, resolution in cryo-EM density maps of icosahedral particles is known to diminish as a function of decreasing radius because of noise that persists along and near the symmetry axes, all of which converge at the particle center.

Averaging of Quasiequivalent μ1-σ3 Heterohexamers

Densities for the R, S, and T heterohexamers were averaged together, first by translating the R and S heterohexamers to the icosahedral 3-fold axis position occupied by the T heterohexamer. Two initial matrices for producing these transformations were calculated from the atomic model of the virion by using the programs Lsq_explicit and Lsq_improve, which are part of the O package (http://xray.bmc.uu.se/~alwyn). For each matrix, the refined coordinates of only one μ1 subunit from each of the R and S heterohexamers were used. The program IMP of the Uppsala software package (Kleywegt and Read, 1997) was then used with the experimental cryo-EM densities for each of the R, S, and T μ1 trimers to obtain a refined pair of matrices. The program MAMA (Kleywegt and Jones, 1999) was used to generate a density mask (extended radius of 6 Å) for each μ1 trimer that is required by the IMP program. We next translated and rotated the densities for the R and S heterohexamers into the position of the T heterohexamer as specified by the matrices refined by IMP. Lastly, the R and S heterohexamer densities were subjected to 3-fold rotational averaging, and the resulting R, S, and T heterohexamer densities were summed to produce the final, averaged map. Each identical monomer within the resulting heterohexamer represents an average of seven unique subunits from the asymmetric unit of the reovirus outer capsid. Density for the σ3 subunit was automatically averaged during this procedure since each unique σ3 is paired with a unique μ1 in the different heterohexamers. Qualitative inspection of the resulting heterohexamer average indicates that the σ3 density is well resolved, providing evidence that μ1-σ3 interactions in the different unique μ1-σ3 pairs are nearly identical and that the same averaging procedure is therefore valid for both μ1 and σ3.

To obtain an estimate of the final resolution of the μ1 subunit in the averaged heterohexamer, the averaging procedure was performed on two independent virion maps. Each independent μ1 average was then extracted within a cube of dimension 60 pixels (133 Å), and the densities outside a sphere of 48 pixel (107 Å) diameter were multiplied with a cosine-like function to attenuate them smoothly to zero. Resolution was then determined in the standard manner by computing and comparing the Fourier transforms of the two cubes of density via Fourier shell crosscorrelation (Baker et al., 1999). The final averaged map of μ1 was computed to a resolution limit of 6.0 Å, by using an inverse temperature factor of 1/350 Å^2 to enhance the high-resolution features out to 6.4 Å, after which the inverse factor was held constant and a Gaussian function was applied to smoothly attenuate the Fourier data to zero from 6.4–6.0 Å.

Fitting of X-Ray Models into the Virion Reconstruction and μ1-σ3 Heterohexamer Average

X-ray crystal models of the μ1-σ3 heterohexamer (PDB entry 1JMU); λ1, σ2, and λ2 subunits within the core particle (PDB entry 1EJ6); and λ3 monomer (PDB entry 1N35) (Liemann et al., 2002; Reinisch et al., 2000; Tao et al., 2002) were fitted into the virion reconstruction. For the 7.6 Å data, the fitting process was carried out with the programs EMfit (Rossmann et al., 2001) and SITUS (Chacón and Wriggers, 2002) as described (Zhang et al., 2003). The results of this earlier fitting formed the starting point for individually refining the fits of 27 subunits—two λ1, three σ2, one λ2, one λ3, ten μ1, and ten σ3—into the 7.0 Å map by using the program Colores of the SITUS package (Chacón and Wriggers, 2002). The densities for each subunit, plus all densities within 20 Å of the subunit, were first extracted by using the program Mapmask in the CCP4 package (CCP4, 1994). Colores was then executed with the search ranges of three Euler angles confined to a 12° window (angular step size of 0.25°) and with the translational search performed at a step size of 0.25 pixels (0.55 Å). The same procedures were used to refine the fits of the μ1 and σ3 subunits into the averaged heterohexamer map.

Contact Residues and Buried Surfaces

Residues in contact (4.0 Å threshold) between subunits were identified in the new atomic model of the virion by using the program CNS (Brünger et al., 1998). The program VIPER (Reddy et al., 2001) was used to estimate the buried surface area between pairs of subunits in the atomic model.

Acknowledgments

This work was supported in part by National Institutes of Health R01 grants to S.C.H. (GM62580 and CA13202), M.L.N. (AI46440 and AI47904), and T.S.B. (GM33050); National Science Foundation (NSF) grants to D.C.M. and T.S.B. (MCB9527131 and DBI0296107); a shared equipment grant from NSF to T.S.B. (BIR 9112921); and a Keck Foundation award and a Purdue University reinvestment grant to the Purdue Structural Biology group. S.C.H. is an investigator of the Howard Hughes Medical Institute. L.Z. received additional support from the Helen Hay Whitney Foundation. We thank M.A. Agosto, J.S.L. Parker, and L.A. Schiff for helpful comments on the manuscript and W. Zhang, C. Xiao, R. Ashmore, X. Yan, and M. Sherman for helpful discussions. The micrographs used in this study, and also to compute the previous 7.6 Å reconstruction, were recorded in part by S.B. Walker and P.R. Chipman.

Received: April 6, 2005
Revised: July 14, 2005
Accepted: July 16, 2005
Published: October 11, 2005

References

Attoui, H., Fang, Q., Jaafar, F.M., Cantaloube, J.F., Biagini, P., De Micco, P., and De Lamballerie, X. (2002). Common evolutionary origin of aquareoviruses and orthoreoviruses revealed by genome characterization of Golden shiner reovirus, Grass carp reovirus, Striped bass reovirus and golden ide reovirus (genus *Aquareovirus*, family Reoviridae). J. Gen. Virol. *83*, 1941–1951.

Baker, T.S., Olson, N.H., and Fuller, S.D. (1999). Adding the third dimension to virus life cycles: three-dimensional reconstruction of icosahedral viruses from cryo-electron micrographs. Microbiol. Mol. Biol. Rev. *63*, 862–922.

Brünger, A.T., Adams, P.D., Clore, G.M., DeLano, W.L., Gros, P., Grosse-Kunstleve, R.W., Jiang, J.S., Kuszewski, J., Nilges, M., Pannu, N.S., et al. (1998). Crystallography & NMR system: a new software suite for macromolecular structure determination. Acta Crystallogr. D Biol. Crystallogr. *54*, 905–921.

CCP4 (Collaborative Computational Project, Number 4) (1994). The CCP4 suite: programs for protein crystallography. Acta Crystallogr. D Biol. Crystallogr. *50*, 760–763.

Chacón, P., and Wriggers, W. (2002). Multi-resolution contour-based fitting of macromolecular structures. J. Mol. Biol. *317*, 375–384.

Chandran, K., and Nibert, M.L. (2003). Animal cell invasion by a large nonenveloped virus: reovirus delivers the goods. Trends Microbiol. *11*, 374–382.

Chandran, K., Walker, S.B., Chen, Y., Contreras, C.M., Schiff, L.A., Baker, T.S., and Nibert, M.L. (1999). In vitro recoating of reovirus cores with baculovirus-expressed outer-capsid proteins μ1 and σ3. J. Virol. *73*, 3941–3950.

Chandran, K., Zhang, X., Olson, N.O., Walker, S.B., Chappell, J.D., Dermody, T.S., Baker, T.S., and Nibert, M.L. (2001). Complete in vitro assembly of the reovirus outer capsid produces highly infectious particles suitable for genetic studies of the receptor-binding protein. J. Virol. *75*, 5335–5342.

Chandran, K., Farsetta, D.L., and Nibert, M.L. (2002). Strategy for nonenveloped virus entry: a hydrophobic conformer of reovirus penetration protein μ1 mediates membrane disruption. J. Virol. *76*, 9920–9933.

Chandran, K., Parker, J.S.L., Ehrlich, M., Kirchhausen, T., and Nibert, M.L. (2003). The δ region of outer-capsid protein μ1 undergoes conformational change and release from reovirus particles during cell entry. J. Virol. *77*, 13361–13375.

Chappell, J.D., Porta, A.E., Dermody, T.S., and Stehle, T. (2002). Crystal structure of reovirus attachment protein σ1 reveals evolutionary relationship to adenovirus fiber. EMBO J. *21*, 1–11.

Dryden, K.A., Wang, G., Yeager, M., Nibert, M.L., Coombs, K.M., Furlong, D.B., Fields, B.N., and Baker, T.S. (1993). Early steps in reovirus infection are associated with dramatic changes in supramolecular structure and protein conformation: analysis of virions and subviral particles by cryoelectron microscopy and image reconstruction. J. Cell Biol. *122*, 1023–1041.

Dryden, K.A., Farsetta, D.L., Wang, G., Keegan, J.M., Fields, B.N., Baker, T.S., and Nibert, M.L. (1998). Internal structures containing transcriptase-related proteins in top component particles of mammalian orthoreovirus. Virology *245*, 33–46.

Farsetta, D.L., Chandran, K., and Nibert, M.L. (2000). Transcriptional activities of reovirus RNA polymerase in recoated cores. Initiation and elongation are regulated by separate mechanisms. J. Biol. Chem. *275*, 39693–39701.

Forrest, J.C., and Dermody, T.S. (2003). Reovirus receptors and pathogenesis. J. Virol. *77*, 9109–9115.

Fotin, A., Cheng, Y., Sliz, P., Grigorieff, N., Harrison, S.C., Kirchhausen, T., and Walz, T. (2004). Molecular model for a complete clathrin lattice from electron cryomicroscopy. Nature *432*, 573–579.

Furlong, D.B., Nibert, M.L., and Fields, B.N. (1988). Sigma 1 protein of mammalian reoviruses extends from the surfaces of viral particles. J. Virol. *62*, 246–256.

Furuichi, Y., and Shatkin, A.J. (2000). Viral and cellular mRNA capping: past and prospects. Adv. Virus Res. *55*, 135–184.

Havelka, W.A., Henderson, R., and Oesterhelt, D. (1995). Three-dimensional structure of halorhodopsin at 7 Å resolution. J. Mol. Biol. *247*, 726–738.

Henderson, R. (2004). Realising the potential of electron cryomicroscopy. Q. Rev. Biophys. *37*, 3–13.

Ji, Y., Marinescu, D.C., Zhang, W., Zhang, X., Yan, X., and Baker, T.S. (2005) A model-based parallel origin and orientation refinement algorithm for cryoTEM and its application to the study of virus structures. J. Struct. Biol., in press.

Jiang, W., Li, Z., Zhang, Z., Baker, M.L., Prevelige, P.E., Jr., and Chiu, W. (2003). Coat protein fold and maturation transition of bacteriophage P22 seen at subnanometer resolutions. Nat. Struct. Biol. *10*, 131–135.

Kim, J., Tao, Y., Reinisch, K.M., Harrison, S.C., and Nibert, M.L. (2004). Orthoreovirus and Aquareovirus core proteins: conserved enzymatic surfaces, but not protein-protein interfaces. Virus Res. *101*, 15–28.

Kleywegt, G.J., and Jones, T.A. (1999). Software for handling mac-

romolecular envelopes. Acta Crystallogr. D Biol. Crystallogr. *55*, 941–944.

Kleywegt, G.J., and Read, R.J. (1997). Not your average density. Structure *5*, 1557–1569.

Lee, P.W., Hayes, E.C., and Joklik, W.K. (1981). Characterization of anti-reovirus immunoglobulins secreted by cloned hybridoma cell lines. Virology *108*, 134–146.

Liemann, S., Chandran, K., Baker, T.S., Nibert, M.L., and Harrison, S.C. (2002). Structure of the reovirus membrane-penetration, μ1, in a complex with its protector protein, σ3. Cell *108*, 283–295.

Luongo, C.L., Zhang, X., Walker, S.B., Chen, Y., Broering, T.J., Farsetta, D.L., Bowman, V.D., Baker, T.S., and Nibert, M.L. (2002). Loss of activities for mRNA synthesis accompanies loss of λ2 spikes from reovirus cores: an effect of λ2 on λ1 shell structure. Virology *296*, 24–38.

Lynch, R.E., Marinescu, D.C., Lin, H., and Baker, T.S. (1999). Parallel algorithms for 3D reconstruction of asymmetric objects from electron micrographs. 13th International Parallel Processing Symposium/10th Symposium on Parallel and Distributed Processing (San Juan, Puerto Rico), pp. 632–637.

Marinescu, D.C., Ji, Y., and Lynch, R.E. (2001). Space-time tradeoffs for parallel 3D reconstruction algorithms for virus structure determination. Concurrency and Computation. Practice & Experience *13*, 1083–1106.

Mendez, I.I., She, Y.M., Ens, W., and Coombs, K.M. (2003). Digestion pattern of reovirus outer capsid protein σ3 determined by mass spectrometry. Virology *311*, 289–304.

Metcalf, P., Cyrklaff, M., and Adrian, M. (1991). The three-dimensional structure of reovirus obtained by cryo-electron microscopy. EMBO J. *10*, 3129–3136.

Middleton, J.K., Severson, T.F., Chandran, K., Gillian, A.L., Yin, J., and Nibert, M.L. (2002). Thermostability of reovirus disassembly intermediates (ISVPs) correlates with genetic, biochemical, and thermodynamic properties of major surface protein μ1. J. Virol. *76*, 1051–1061.

Nason, E.L., Wetzel, J.D., Mukherjee, S.K., Barton, E.S., Prasad, B.V.V., and Dermody, T.S. (2001). A monoclonal antibody specific for reovirus outer-capsid protein σ3 inhibits σ1-mediated hemagglutination by steric hindrance. J. Virol. *75*, 6625–6634.

Nibert, M.L. (1993). Structure and function of reovirus outer capsid proteins as they relate to early steps in infection. PhD thesis, Harvard University, Cambridge, Massachusetts.

Nibert, M.L., Furlong, D.B., and Fields, B.N. (1991a). Mechanisms of viral pathogenesis. Distinct forms of reoviruses and their roles during replication in cells and host. J. Clin. Invest. *88*, 727–734.

Nibert, M.L., Schiff, L.A., and Fields, B.N. (1991b). Mammalian reoviruses contain a myristoylated structural protein. J. Virol. *65*, 1960–1967.

Nibert, M.L., Odegard, A.L., Agosto, M.A., Chandran, K., and Schiff, L.A. (2005). Putative autocleavage of reovirus μ1 protein in concert with outer-capsid disassembly and activation for membrane permeabilization. J. Mol. Biol. *345*, 461–474.

Noad, L., Shou, J., Coombs, K.M., and Duncan, R. (2005). Sequences of avian reovirus M1, M2, and M3 genes and structural function of the encoded μ proteins. Virus, in press.

Odegard, A.L., Chandran, K., Liemann, S., Harrison, S.C., and Nibert, M.L. (2003). Disulfide bonding among μ1 trimers in mammalian reovirus outer capsid: a late and reversible step in virion morphogenesis. J. Virol. *77*, 5389–5400.

Odegard, A.L., Chandran, K., Zhang, X., Parker, J.S.L., Baker, T.S., and Nibert, M.L. (2004). Putative autocleavage of outer capsid protein μ1, allowing release of myristoylated peptide μ1N during particle uncoating, is critical for cell entry by reovirus. J. Virol. *78*, 8732–8745.

Reddy, V.S., Natarajan, P., Okerberg, B., Li, K., Damodaran, K.V., Morton, R.T., Brooks, C.L., 3rd, and Johnson, J.E. (2001). Virus Particle Explorer (VIPER), a website for virus capsid structures and their computational analyses. J. Virol. *75*, 11943–11947.

Reinisch, K.M., Nibert, M.L., and Harrison, S.C. (2000). Structure of the reovirus core at 3.6 Å resolution. Nature *404*, 960–967.

Rosenthal, P.B., and Henderson, R. (2003). Optimal determination of particle orientation, absolute hand, and contrast loss in single-particle electron cryomicroscopy. J. Mol. Biol. *333*, 721–745.

Rossmann, M.G., Bernal, R., and Pletnev, S.V. (2001). Combining electron microscopic with X-ray crystallographic structures. J. Struct. Biol. *136*, 190–200.

Sharpe, A.H., and Fields, B.N. (1985). Pathogenesis of viral infections. Basic concepts derived from the reovirus model. N. Engl. J. Med. *312*, 486–497.

Shing, M., and Coombs, K.M. (1996). Assembly of the reovirus outer capsid requires μ1/σ3 interactions which are prevented by misfolded σ3 protein in temperature-sensitive mutant tsG453. Virus Res. *46*, 19–29.

Smith, R.E., Zweerink, H.J., and Joklik, W.K. (1969). Polypeptide components of virions, top component and cores of reovirus type 3. Virology *39*, 791–810.

Tao, Y., Farsetta, D.L., Nibert, M.L., and Harrison, S.C. (2002). RNA synthesis in a cage—structural studies of the reovirus polymerase λ3. Cell *111*, 733–745.

Tillotson, L., and Shatkin, A.J. (1992). Reovirus polypeptide σ3 and N-terminal myristoylation of polypeptide μ1 are required for site-specific cleavage to μ1C in transfected cells. J. Virol. *66*, 2180–2186.

Tyler, K.L., Clarke, P., DeBiasi, R.L., Kominsky, D., and Poggioli, G.J. (2001). Reoviruses and the host cell. Trends Microbiol. *9*, 560–564.

Wilson, G.J., Nason, E.L., Hardy, C.S., Ebert, D.H., Wetzel, J.D., Prasad, B.V.V., and Dermody, T.S. (2002). A single mutation in the carboxy terminus of reovirus outer-capsid protein σ3 confers enhanced kinetics of σ3 proteolysis, resistance to inhibitors of viral disassembly, and alterations in σ3 structure. J. Virol. *76*, 9832–9843.

Zhang, X., Walker, S.B., Chipman, P.R., Nibert, M.L., and Baker, T.S. (2003). Reovirus polymerase λ3 localized by cryo-electron microscopy of virions at a resolution of 7.6 Å. Nat. Struct. Biol. *10*, 1011–1018.

Zhou, Z.H., Dougherty, M., Jakana, J., He, J., Rixon, F.J., and Chiu, W. (2000). Seeing the herpesvirus capsid at 8.5 Å. Science *288*, 877–880.

Zhou, Z.H., Baker, M.L., Jiang, W., Dougherty, M., Jakana, J., Dong, G., Lu, G., and Chiu, W. (2001). Electron cryomicroscopy and bioinformatics suggest protein fold models for rice dwarf virus. Nat. Struct. Biol. *8*, 868–873.

Accession Numbers

The atomic coordinates of the structures have been deposited in the Protein Data Bank under code 2CSE.